Structural insights into the regulation of sialic acid catabolism by the *Vibrio vulnificus* transcriptional repressor NanR

Jungwon Hwang[a,b,1], Byoung Sik Kim[c,1], Song Yee Jang[a], Jong Gyu Lim[c], Dong-Ju You[d], Hyun Suk Jung[d], Tae-Kwang Oh[a], Jie-Oh Lee[b], Sang Ho Choi[c,2], and Myung Hee Kim[a,e,2]

[a]Infection and Immunity Research Center, Korea Research Institute of Bioscience and Biotechnology, Daejeon 305-806, Korea; [b]Department of Chemistry, Korea Advanced Institute of Science and Technology, Daejeon 305-701, Korea; [c]National Research Laboratory of Molecular Microbiology and Toxicology, Department of Agricultural Biotechnology, Center for Food Safety and Toxicology, Seoul National University, Seoul 151-921, Korea; [d]Division of Electron Microscopic Research, Korea Basic Science Institute, Daejeon 305-333, Korea; and [e]Biosystems and Bioengineering Program, University of Science and Technology, Daejeon 305-350, Korea

Edited by Robert Huber, Max Planck Institute of Biochemistry, Planegg-Martinsried, Germany, and approved June 6, 2013 (received for review February 16, 2013)

Pathogenic and commensal bacteria that experience limited nutrient availability in their host have evolved sophisticated systems to catabolize the mucin sugar *N*-acetylneuraminic acid, thereby facilitating their survival and colonization. The correct function of the associated catabolic machinery is particularly crucial for the pathogenesis of enteropathogenic bacteria during infection, although the molecular mechanisms involved with the regulation of the catabolic machinery are unknown. This study reports the complex structure of NanR, a repressor of the *N*-acetylneuraminate (*nan*) genes responsible for *N*-acetylneuraminic acid catabolism, and its regulatory ligand, *N*-acetylmannosamine 6-phosphate (ManNAc-6P), in the human pathogenic bacterium *Vibrio vulnificus*. Structural studies combined with electron microscopic, biochemical, and in vivo analysis demonstrated that NanR forms a dimer in which the two monomers create an arched tunnel-like DNA-binding space, which contains positively charged residues that interact with the *nan* promoter. The interaction between the NanR dimer and DNA is alleviated by the ManNAc-6P–mediated relocation of residues in the ligand-binding domain of NanR, which subsequently relieves the repressive effect of NanR and induces the transcription of the *nan* genes. Survival studies in which mice were challenged with a ManNAc-6P–binding-defective mutant strain of *V. vulnificus* demonstrated that this relocation of NanR residues is critical for *V. vulnificus* pathogenesis. In summary, this study presents a model of the mechanism that regulates sialic acid catabolism via NanR in *V. vulnificus*.

nan gene repressor | mucin sugar utilization

Pathogenic bacteria that colonize the host gut are exposed to an adverse environment and competitors (1, 2). These bacteria overcome the limited availability of nutrients in the gut (3) by using alternative carbon sources (4). The mammalian intestinal tract is protected by a mucus layer, which contains heavily glycosylated mucin proteins that comprise up to 85% carbohydrate (5, 6). Sialic acids, which can be used as an energy source by a variety of microbial pathogens and commensals, are found at the distal ends of the mucin carbohydrate chains (7, 8). Because the most abundant sialic acid is *N*-acetylneuraminic acid (Neu5Ac) (7–9), intestinal commensal and pathogenic bacteria have most likely evolved elaborate systems for the catabolic utilization of this substrate.

Escherichia coli, *Vibrio cholerae*, *Vibrio vulnificus*, and *Staphylococcus aureus* can grow by using Neu5Ac as a sole carbon source (10–13), and the *N*-acetylneuraminate (*nan*) genes responsible for Neu5Ac utilization are up-regulated during their growth on mucus or in the mammalian intestine (3, 14). The colonization and pathogenic activities of these bacteria are affected severely by mutations in the *nan* genes (3, 12, 15). This phenotype suggests that the correct expression and function of the proteins responsible for Neu5Ac catabolism are essential for the growth and survival of enteric bacteria, although only a few studies have investigated the regulatory mechanisms of *nan* genes. *E. coli* requires the *nanATEK* operon to catabolize Neu5Ac (16). *E. coli* NanR ($NanR_{Ec}$) is a repressor of this operon, and the displacement of $NanR_{Ec}$ by Neu5Ac (*SI Appendix*, Fig. S1) leads to the expression of the operon (17). *Haemophilus influenzae* employs the *nan* and *siaPT* operons to catabolize Neu5A (18), and these operons are repressed by SiaR, whereas glucosamine 6-phosphate (GlcN-6P; *SI Appendix*, Fig. S1), which is the catabolic intermediate of Neu5Ac, functions as a coactivator of SiaR (19). However, the molecular mechanisms that govern the repression or activation of these operons have not been studied.

The foodborne enteropathogen *V. vulnificus*, which usually enters the body as a contaminant of raw seafood, causes gastroenteritis and life-threatening septicemia in immunocompromised individuals. Before entering the bloodstream, *V. vulnificus*

Significance

Pathogenic bacteria that experience limited nutrient availability in the host gut have evolved sophisticated systems to catabolize *N*-acetylneuraminic acid (Neu5Ac; sialic acid). This study reports the structural analysis of NanR, a repressor of the *N*-acetylneuraminate (*nan*) genes responsible for Neu5Ac catabolism, complexed with its regulatory ligand, *N*-acetylmannosamine 6-phosphate (ManNAc-6P). The interaction between NanR and the *nan* promoter is alleviated by the ManNAc-6P–mediated relocation of residues in the ligand-binding domain of NanR, which subsequently relieves the repressive effect of NanR and induces the transcription of *nan* genes. These events are required for survival and for *Vibrio vulnificus* pathogenesis.

Author contributions: J.H., B.S.K., S.H.C., and M.H.K. designed research; J.H., B.S.K., S.Y.J., J.G.L., D.-J.Y., H.S.J., and M.H.K. performed research; T.-K.O. and J.-O.L. contributed new reagents/analytic tools; J.H., B.S.K., S.Y.J., J.G.L., D.-J.Y., H.S.J., S.H.C., and M.H.K. analyzed data; and J.H., B.S.K., S.H.C., and M.H.K. wrote the paper.

The authors declare no conflict of interest.

This article is a PNAS Direct Submission.

Freely available online through the PNAS open access option.

Data deposition: The atomic coordinates and structure factors have been deposited in the Protein Data Bank, www.pdb.org (PDB ID code 4IVN).

[1]J.H. and B.S.K. contributed equally to this work.

[2]To whom correspondence may be addressed. E-mail: mhk8n@kribb.re.kr or choish@snu.ac.kr.

This article contains supporting information online at www.pnas.org/lookup/suppl/doi:10.1073/pnas.1302859110/-/DCSupplemental.

colonizes the small intestine. Recently, we demonstrated that *V. vulnificus* NanR is a transcriptional repressor of the *nanT*$_{PSL}$*AR* (the operon consisting of the genes encoding *V. vulnificus* Neu5Ac tripartite ATP-independent periplasmic transporter, Neu5Ac aldolase and *nan* gene repressor) and *nanEK* [the operon consisting of the genes encoding *N*-acetylmannosamine 6-phosphate (ManNAc-6P) epimerase and ManNAc kinase] *nagA* (the gene encoding *N*-acetylglucosamine 6-phosphate deaminase) operons (20). We also showed that ManNAc-6P (*SI Appendix*, Fig. S1), the catabolic intermediate of Neu5Ac, binds specifically to NanR and induces the expression of *nan* genes (20). However, the molecular mechanisms that underlie the regulation of *nan* genes by NanR and ManNAc-6P are unknown. Thus, the present study analyzed the structure of the NanR/ManNAc-6P complex and investigated the regulation of *nan* genes by this complex by using in vitro and in vivo assays, as well as electron microscopy. Furthermore, this study highlights the relationship between *V. vulnificus* pathogenesis and the control of *nan* genes by NanR and its regulatory ligand.

Results

Structure of the NanR/ManNAc-6P Complex. The NanR/ManNAc-6P complex was crystallized, and its structure was determined by using the single anomalous wavelength dispersion and molecular replacement methods. The structure was refined to a resolution of 1.9 Å (Table 1). In contrast to the typical structure of other transcriptional regulators, the NanR/ManNAc-6P complex contains two molecules in an asymmetric unit (*SI Appendix*, Fig. S2*A*). The symmetry mates were analyzed in the dimer, and a functional dimeric form of NanR was confirmed by electron microscopy (*SI Appendix*, Fig. S2*B*; *Electron Microscopic Analysis of the Interaction Between NanR and the* nan *Operator*). The two NanR molecules in the dimer face each other and are tilted ∼45° in opposite directions (Fig. 1*A*). NanR has a two-domain architecture with an N-terminal DNA-binding domain (DBD) and a large C-terminal ligand-binding domain (LBD) (Fig. 1*B*). The DBD comprises six α-helices, whereas the LBD forms an α/β structure, which is characterized as a five-stranded parallel β-sheet flanked by α-helices on both sides (Fig. 1*B*). The residues between α6 and α7 were not included in the final model because they were invisible in the electron density map; these regions are probably highly flexible. A DALI search showed that no structures similar to that of NanR have been published. However, the structure of the LBD resembles the isomerase domain of glucosamine-6-phosphate synthase (GlmS), a bienzyme complex that catalyzes the first step during hexosamine metabolism (21). The fructose 6-phosphate binding site in the N-terminal isomerase subdomain of GlmS is located in the same position as the ManNAc-6P binding site in the NanR LBD, which suggests that NanR has evolutionarily adapted the isomerase domain to sense the *nan* regulatory molecule, which has a similar structure to fructose 6-phosphate. The structure of the NanR DBD is similar to the N-terminal domain of the *Bacillus subtilis* putative transcriptional regulator ybbH [Protein Data Bank (PDB) ID code 2O3F]. ManNAc-6P is located at the C-terminal edge of the β-sheet in the LBD (Fig. 1*B*).

Characterization of the Interaction Between ManNAc-6P and NanR. An electron density difference map showed that ManNAc-6P binds to NanR via the site formed by the L9, L13, and L17 loops of the LBD (Fig. 2*A*). L13, which corresponds to the P loop in the GlmS isomerase subdomain, crosses over and loops around the phosphate group of ManNAc-6P (Fig. 2 *A* and *B*). The phosphate oxygen atoms form hydrogen bonds with the side chains of S182, S184, and T187 and with the backbone amide of

Table 1. Data collection and refinement statistics for NanR complexed with ManNAc-6P

Dataset	SeMet–NanR complexed with ManNAc-6P	NanR complexed with ManNAc-6P
Wavelength	0.97917	1.0000
Space group	$P3_121$	$P3_121$
Unit cell, Å	$a = b = 109.84$, $c = 83.38$ $\alpha = \beta = 90°$, $\gamma = 120°$	$a = b = 109.21$, $c = 82.47$ $\alpha = \beta = 90°$, $\gamma = 120°$
Resolution, Å	50.0–2.40 (2.49–2.40)	50.0–1.90 (1.93–1.90)
No. of total reflections	508,845	330,826
No. of unique reflections	23,076	45,033
Redundancy	22.1 (22.47)	7.3 (7.3)
Completeness, %	99.9 (100.0)	99.9 (100.0)
R_{sym},* %	9.4 (31.5)	4.7 (47.3)
$I/\sigma(I)$	50.27 (12.28)	42.05 (3.15)
Refinement		
Resolution, Å		30.0–1.90
Reflections in work/test sets		42,737/2,268
R_{work}/R_{free},†‡ %		18.3/23.5
rms deviations		
Bond lengths, Å		0.021
Bond angles, °		2.126
Model composition		
		525 residues 221 waters 2 ManNAc-6P
Geometry		
Favored regions, %		98.8
Allowed regions, %		1.2
PDB ID code		4IVN

The numbers in parentheses indicate the relevant values for the highest resolution shell.
*$R_{sym} = \Sigma|I_i - <I>|/\Sigma I$ where I_i is the intensity of the ith observation, and $<I>$ is the mean intensity of the reflections.
†$R_{work} = \Sigma||F_{obs}| - |F_{calc}||/\Sigma|F_{obs}|$ where F_{calc} and F_{obs} are the calculated and observed structure factor amplitude, respectively.
‡$R_{free} = \Sigma||F_{obs}| - |F_{calc}||/\Sigma|F_{obs}|$ where all reflections belong to a test set of randomly selected data.

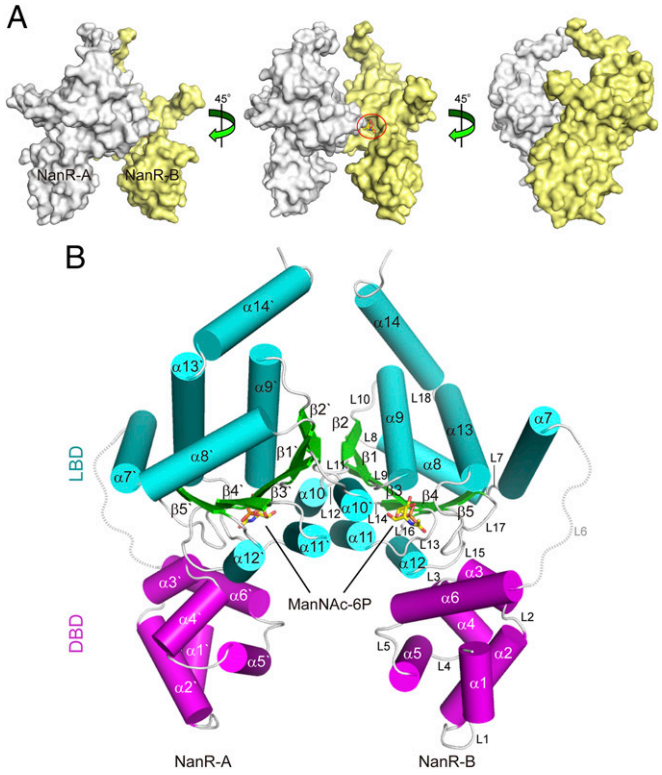

Fig. 1. Overall structure of the NanR/ManNAc-6P complex. (*A*) Surface representation of the NanR/ManNAc-6P complex, which shows that the two NanR molecules face each other while tilting in opposite directions. The ligand-binding site is indicated by a red circle. (*B*) Ribbon representation of the NanR/ManNAc-6P complex in its dimeric form. NanR comprises an N-terminal DNA-binding domain (DBD) and a C-terminal ligand-binding domain (LBD). The α-helices and β-sheets of the LBD are shown in cyan and green, respectively. The α-helices of the DBD are shown in magenta. The position of ManNAc-6P is indicated in each NanR molecule.

S183 in the P loop (Fig. 2 *B*, *Upper*). This binding structure is very similar to that of GlmS isomerase (Fig. 2 *B*, *Lower*). The side-chain hydroxyl group of S138 in L9 is also hydrogen-bonded to a ManNAc-6P phosphate oxygen atom (Fig. 2 *A* and *B*). The hydroxyl group in position O4 of the sugar ring forms a hydrogen bond with the A137 backbone amide. A hand-in-hand interaction is formed between the two NanR monomers by hydrogen bonds between the hydroxyl group at position O1 of the sugar ring in each NanR monomer and the nitrogen atom in the imidazole ring of each H163 (Fig. 2 *A* and *C*). This structure is critical for the conformational change in the NanR dimer and the delivery of the signal to the *nan* operon genes when ligand binding occurs. Furthermore, the phosphoryl group of the ligand forms a water-mediated hydrogen bond with the side-chain amino group of R71 on α6 in the DBD (Fig. 2 *A* and *C*). These interactions may facilitate the ligand-mediated relocation of the NanR dimer and influence its interaction with the *nan* operator. P231 and G234 form water-mediated hydrogen bonds with the carbonyl oxygen atom of the *N*-acetyl group (Fig. 2*A*). E229 and K240 also form water-mediated hydrogen bonds with the sugar and phosphate oxygen atoms of ManNAc-6P (Fig. 2*A*).

To assess the importance of the interaction between ManNAc-6P and NanR during the regulation of *nan* genes, the residues involved in ligand binding were mutated, and their effects on the function of NanR were investigated by using an *E. coli* dual plasmid system (22). Cells were cotransformed with plasmids that contained a luciferase reporter gene fused to the NanR-binding *nanT*$_{PSL}$*AR* promoter (P$_{nanTp}$) and wild-type (WT) or mutant NanR, followed by incubation in the presence of arabinose and in the presence or absence of Neu5Ac. The luciferase activity increased in cells that expressed WT NanR after the addition of Neu5Ac, whereas Neu5Ac was unable to activate P$_{nanTp}$ in cells that expressed the S138A, H163A, H163L, S182A, E229L, K240A, or K240M mutants, but not the S184A and T187A mutants (Fig. 2*D*). These results suggest that the precise binding of ManNAc-6P, the metabolic intermediary of Neu5Ac to NanR, is critical for the regulation of *nan* genes.

Characterization of the DBD of NanR. The simplest helix–turn–helix (HTH)-containing DBD comprises three core helices. The HTH domains can form tetra-helical bundles, winged helices, and ribbon–helix–helix-type configurations (23). The DBD of NanR is a six-helix bundle, which is not the archetypal conformation of HTH-containing domains. Therefore, the recognition helix required for DNA binding could not be determined. However, analysis of the surface electrostatic potential of NanR identified a number of positively charged residues in the DBD, including K20, K21, R23, R57, R60, and K65, which may be responsible for binding to the phosphate backbone of DNA (Fig. 3 *A* and *B*). The importance of these residues during DNA binding was tested by using an *E. coli* dual plasmid system, as described above. The repressive effect of WT NanR on the activity of P$_{nanTp}$ was abolished by the R57A, R57L, R60A, and R60L point mutations (Fig. 3*C*). Western blot analyses using anti-NanR antiserum showed that these results were attributable to the functional defects of the mutants rather than reduced cellular expression (*SI Appendix*, Fig. S3).

NanR represses the *nanT*$_{PSL}$*AR* and *nanEK nagA* operons by binding to an operator within the *nanT*$_p$–*nanE* intergenic region (20). To examine further the role of R57 and R60 in DNA binding, electrophoretic gel mobility shift assays (EMSAs) were performed in which the *nanT*$_p$–*nanE* intergenic region was incubated with WT or mutant NanR in the absence or presence of ManNAc-6P. The addition of ManNAc-6P relieved the retardation of DNA migration, which suggests that ManNAc-6P affects the ability of NanR to bind to the *nan* operator. The retardation of DNA migration was not detected with the R57A or R60A mutants (Fig. 3*D*). With the exception of the S184A mutant, which had the same activity as WT NanR in the *E. coli* dual-plasmid system experiments (Fig. 2*D*), the DNA migration with the ligand-binding-defective NanR mutants were not affected by the addition of ManNAc-6P (Fig. 3*D*). In addition, an in vitro transcription assay showed that the R57A and R60A mutants did not repress P$_{nanE}$, even in the absence of ManNAc-6P, and they facilitated the transcription of *nanE*, unlike the WT and the S184A mutant (Fig. 3*E*). In agreements with the EMSA results and the *E. coli* dual plasmid system assay, the other ligand-binding-defective NanR mutants did not allow the transcription of *nanE* in the presence or absence of ManNAc-6P (Fig. 3*E*). These results indicate that the R57 and R60 residues in α5 are indispensable for NanR binding to the *nan* operator and that the DNA-binding HTH motif in each NanR monomer comprises α4 and α5. The distance between the two α5 helices in the NanR dimer is ∼22 Å (Fig. 3*B*), which suggests that the method of DNA binding used by NanR differs from that of other HTH motif-containing transcriptional regulators (23).

ManNAc-6P Alleviates the Interaction Between NanR and the *nan* Operator. The EMSA and in vitro transcription experiments demonstrated that S138, H163, S182, E229, and K240 are critical for ligand sensing and the regulation of *nan* genes by NanR. It was hypothesized that the binding of ManNAc-6P may alter the conformation of NanR and alleviate its interaction with the *nan* operator. To test this hypothesis, a DNaseI footprinting assay was performed by using NanR and ^{32}P-labeled *nan* operator DNA. After the addition of ManNAc-6P, the hypersensitive

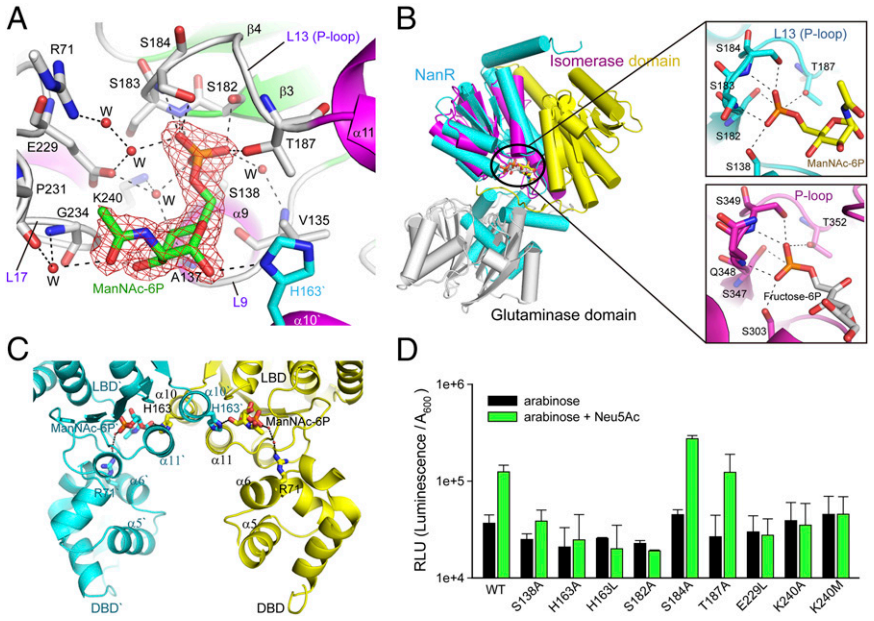

Fig. 2. Structural analysis of the interaction between ManNAc-6P and NanR. (*A*) Electron density difference map showing the position of ManNAc-6P in the ligand-binding site. The $F_o - F_c$ map was calculated before the inclusion of ManNAc-6P and is contoured at 3.5 σ. The residues critical for the interaction between NanR and the ligand are shown, where the carbon atoms are colored gray. The H163 residue with cyan-colored carbon atoms originates from the opposing NanR monomer. (*B*) The structure of NanR (cyan) superimposed onto that of GlmS, which has an isomerase domain (magenta and yellow) and a glutaminase domain (gray). The P-loop–binding ligand of each protein is shown in *Insets*. (*C*) The two NanR monomers have a hand-in-hand interaction that involves hydrogen bonds between the nitrogen atom in the imidazole ring of each H163 and the sugar hydroxyl group of each ligand. R71 in the α6 helix of the DBD forms a water-mediated hydrogen bond with the phosphoryl group of the ligand. (*D*) Results of an *E. coli* dual plasmid system assay in which cells were cotransformed with a luciferase reporter gene fused to P_{nanTp} and WT or mutant NanR, followed by incubation in the presence (5 mM) or absence of Neu5Ac. The relative luminescence unit (RLU) was calculated by dividing the luminescence by the A_{600} of each strain. The data represent the mean ± SD from at least three experiments.

cleavage bands at the center of the NanR-binding site disappeared, and neighboring regions were deprotected from cleavage (*SI Appendix*, Fig. S4). The isothermal titration calorimetry analyses detected a robust interaction between the NanR dimer and the target DNA, with a 1:1 binding stoichiometry and a dissociation constant (K_d) of 1.40 μM (Fig. 3*F* and *SI Appendix*, Fig. S5*A*). However, the interaction affinity of NanR complexed with ManNAc-6P was reduced 130-fold (K_d = 185.87 μM) (Fig. 3*F* and *SI Appendix*, Fig. S5*B*). Overall, these results support the hypothesis that ManNAc-6P alters the conformation of NanR through relocation of the ligand-binding residues, which alleviates the interaction of NanR with the *nan* operator, thereby leading to the up-regulation of *nan* genes.

Electron Microscopic Analysis of the Interaction Between NanR and the *nan* Operator. Electron microscopy using negative staining followed by single particle analysis showed that apo-NanR and the NanR/ManNAc-6P complex share similar structural features when analyzed at the molecular level with an ∼2-nm resolution (Fig. 4*A* and *SI Appendix*, Fig. S6 *A* and *B*). Additional electron microscopy densities were observed for the DNA-bound NanR dimer (Fig. 4 *A* and *B*, white arrows; *SI Appendix*, Fig. S6*C*). The binding pattern of the DNA showed that it passes between the DBDs in the NanR dimer. Notably, the α5 helix of each NanR molecule is essential for DNA binding. The distance between the α5 helices that project toward the interior of the DBDs is ∼22 Å (Fig. 3*B*), which is close to the width of the DNA double helix (20 Å). A 2D fitting demonstrated that the atomic models assembled from the crystal structures of NanR and DNA (Fig. 4 *B*, *Center*) have a good fit with the averaged image of the NanR/DNA complex (Fig. 4 *B*, *Right*). However, the entire length of the DNA associated with NanR does not match perfectly because of its flexibility. Further inspection of the surface electrostatic potential of α11 in the LBD of NanR identified positively charged residues that may also be responsible for DNA binding (Fig. 4*C*). The importance of the K188 and K199 residues in α11 for the binding of NanR to DNA was assessed by EMSA. The K188A, K188L, K199A, and K199L mutants could bind to DNA, but the binding activities of the mutants were not as conspicuous as that of WT NanR (*SI Appendix*, Fig. S7). Furthermore, the mutants were much more susceptible to ManNAc-6P than WT NanR (*SI Appendix*, Fig. S7).

These results demonstrate that the NanR dimer forms an arched tunnel-like DNA-binding space, which is formed mainly by α5 and α11 in each monomer. The *nan* operator interacts with the dimer through the positively charged residues in this space (Fig. 4 *B* and *C*).

The Interaction Between ManNAc-6P and NanR Is Crucial for Growth and Survival During Infection. The robust control of the genes encoding catabolic enzymes and the putative transporter for Neu5Ac is crucial for the growth and survival of pathogenic bacteria in the host (12, 20). The effects of mutations in R57 and H163—which are critical for DNA binding and ligand binding, respectively—on the growth of the pathogenic bacterium *V. vulnificus* were tested to elucidate the biological relevance of ligand sensing by NanR. The R57A or H163L mutations were introduced into *V. vulnificus* chromosomal DNA, and the in vitro growth of each mutant strain was examined. The growth of the R57A strain was similar to that of the WT strain, whereas the growth of the H163L strain was impaired in minimal M9 medium supplemented with Neu5Ac as the sole carbon source (Fig. 5*A*). The addition of D-xylose and L-proline restored the growth of the H163L strain, which had an altered colony morphotype with reduced opacity (Fig. 5*A*), which was also observed previously with the *nanA* (the gene encoding for Neu5Ac aldolase) mutant

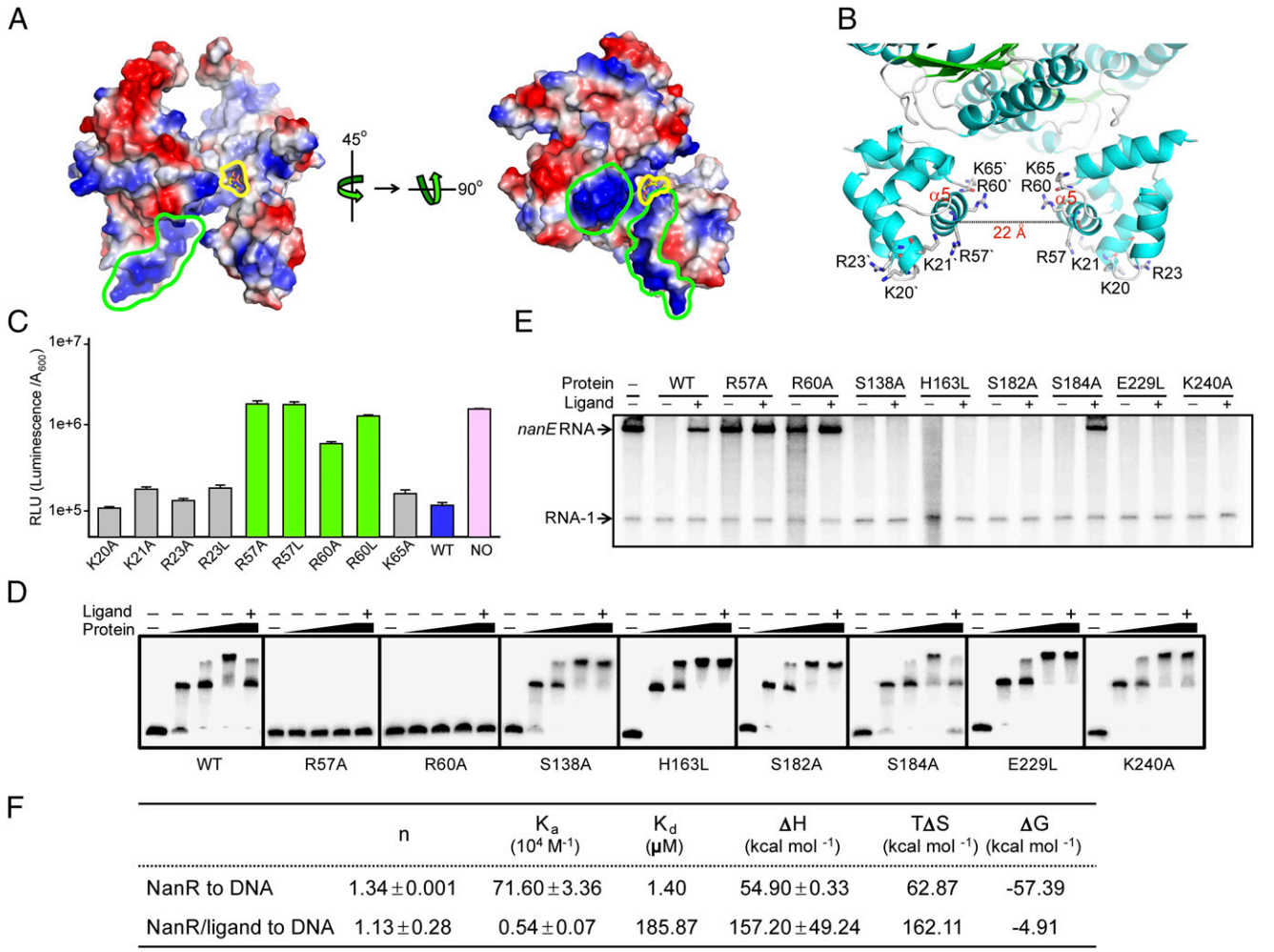

F

	n	K_a (10^4 M^{-1})	K_d (μM)	ΔH (kcal mol $^{-1}$)	TΔS (kcal mol $^{-1}$)	ΔG (kcal mol $^{-1}$)
NanR to DNA	1.34 ± 0.001	71.60 ± 3.36	1.40	54.90 ± 0.33	62.87	-57.39
NanR/ligand to DNA	1.13 ± 0.28	0.54 ± 0.07	185.87	157.20 ± 49.24	162.11	-4.91

Fig. 3. The DNA-binding activity of NanR is regulated by ManNAc-6P. (*A*) Surface electrostatic potential of NanR showing the distribution of positively charged residues (outlined in green) in the DBD. The ligand-binding site is outlined in yellow. (*B*) Position of the positively charged residues in the DBD of each NanR molecule. (*C*) Results of an *E. coli* dual plasmid system assay in which cells were cotransformed with a luciferase reporter gene fused to P_{nanTp} and WT NanR, mutant NanR, or empty vector (NO). The RLU was calculated by dividing the luminescence by the A_{600} of each strain. The data represent the mean ± SD from at least three experiments. (*D*) EMSA analysis of the interaction between the $nanT_p$–*nanE* intergenic region and WT or mutant NanR (protein) in the absence or presence of ManNAc-6P (ligand). (*E*) Results of an in vitro transcription assay in which the supercoiled pBS0921 plasmid containing P_{nanE} was transcribed in the presence or absence of 100 nM WT or mutant NanR (protein) and 1 mM ManNAc-6P (ligand). The 370-bp P_{nanE}-specific transcript and the vector-derived control transcript (RNA-1) are indicated. (*F*) The effect of ManNAc-6P on the interaction between NanR and the *nan* operator, which was determined by using isothermal titration calorimetry.

strain (12). In the medium supplemented with D-xylose, L-proline, and Neu5Ac, the expression levels of the *nan* genes in the H163L mutant were at least 142-fold lower than those in the WT (*SI Appendix*, Fig. S8). These results suggest that the H163L mutant was defective for ManNAc-6P sensing and *nan* gene regulation, which affected the growth of *V. vulnificus* when Neu5Ac was available.

Furthermore, a mouse intestine colonization competition assay was performed to examine the importance of H163 for ligand binding. In 8 of 10 mice, colonization by the H163L mutant strain was 22.4-fold lower than that by the WT strain, which resulted in a median competitive index of 0.045 (Fig. 5*B*). Finally, the mice were challenged with a lethal dose of *V. vulnificus*. At 24 h postinfection, the percentages of mice that survived after challenge with the H163 mutant or WT strain were 80% and 45%, respectively (Fig. 5*C*). These results indicate that the regulation of NanR by ManNAc-6P is required not only for growth and survival, but also for the pathogenesis of *V. vulnificus*.

Discussion

Microorganisms use the exposed sialyl residues on host cell surfaces for adhesive or invasive purposes (24). To avoid host immunity, pathogens such as *H. influenzae* and *Neisseria meningitidis* use acquired or de novo synthesized sialic acid for their surface decoration, i.e., lipopolysaccharide/lipooligosaccharide sialylation (25). The key enzymes involved in these modifications are Neu5Ac synthase (NeuB) and cytidine-5′-monophospho-Neu5Ac synthetase (NeuA), which synthesize and activate Neu5Ac, respectively, to generate cytidine monophosphate (CMP)–Neu5Ac, a precursor of sialyl-conjugates (7) (Fig. 5*D*). In addition, these nine-carbon amino sugars may facilitate bacterial survival and colonization (26). The *nan* genes required to use sialic acids as a nutrient source (Fig. 5*D*) are found only in pathogenic and commensal bacterial species, and this ability is correlated with bacterial virulence (15, 27).

The present study investigated the molecular basis of the regulation of *nan* genes by NanR and its regulatory ligand ManNAc-6P. The results demonstrated that NanR interacts with

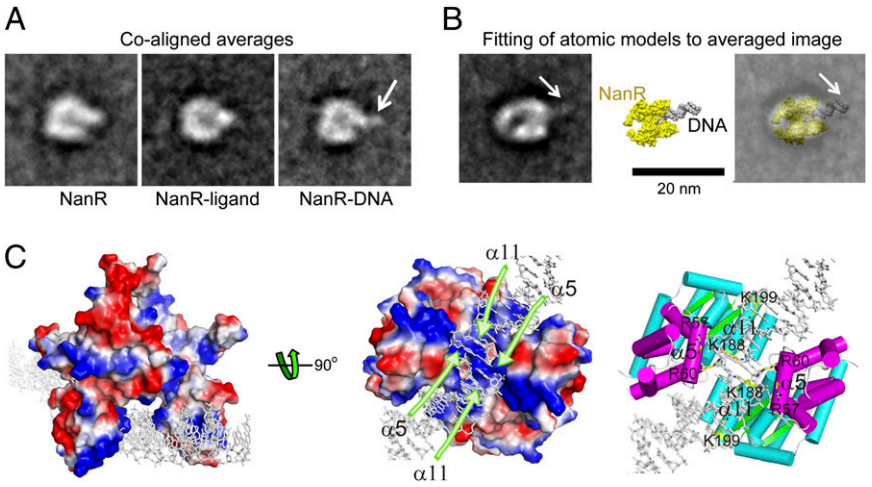

Fig. 4. Electron-microscopic analysis of NanR. (*A*) Selected averaged images of apo-NanR, the NanR/ManNAc-6P complex, and the apo-NanR/DNA complex. Protein samples were negatively stained, and the molecular structures were determined by single particle analysis. The images of three protein samples were grouped, coaligned, and classified based on the main features of the apo-NanR densities. (*B*) The atomic models of NanR and DNA (modified from PDB ID code 2O6G) fitted to the NanR–DNA complex. A representative averaged image of the NanR–DNA complex (the asterisk-marked image in *SI Appendix*, Fig. S6*C*), the equivalent view of the assembled atomic model, and the superposition of the atomic model on the average are shown in *Left*, *Center*, and *Right*, respectively. The white arrows in *A* and *B* indicate the appearance of densities associated with DNA binding. (*C*) The structure of the NanR/DNA complex, which was modeled based on the electron-microscopic analysis and in vivo and in vitro investigations. The R57 and R60 residues in α5 and K188 and K199 in α11, which are required for DNA binding, are indicated.

the *nan* promoter (Fig. 3*F*) through an arched tunnel-like DNA-binding site (Fig. 4). The flexibility of the DBDs in the ligand-free NanR dimer may facilitate the interaction with the *nan* operator. The distance between the DBDs in the ManNAc-6P–bound NanR dimer is 22 Å, which is somewhat narrow given that the width of double-stranded DNA is ∼20 Å. Thus, it is proposed that when *V. vulnificus* experiences limited nutrient availability in the host gut, it absorbs the available Neu5Ac through its membrane-bound NanT transporter (Fig. 5*D*). Next, ManNAc-6P, the catabolic intermediate of Neu5Ac, is produced by NanA and *N*-acetylmannosamine kinase (NanK), and the ligand is sensed by NanR. This event causes the ligand-mediated relocation of residues, which induces a tight dimeric conformation of NanR that affects its interaction with the *nan* operator (Fig. 5*D*). The results of this study suggest that the ligand-mediated hand-in-hand interaction between the two H163 residues in the NanR dimer is required specifically for this event. The alleviation of the repressive effect of NanR by ManNAc-6P—which was demonstrated by using in vitro EMSA (Fig. 3*D*), isothermal titration calorimetry (Fig. 3*F*), and DNaseI footprinting assays (*SI Appendix*, Fig. S4*A*)—may allow RNA polymerase to access the operator region so that it can actively transcribe P_{nanTp} and P_{nanE} (20, 28). Ultimately, these events allow the bacteria to survive and colonize in the host. Indeed, the significantly lower survival of mice after challenge with a ManNAc-6P–binding-defective mutant strain of *V. vulnificus* demonstrated that the binding of ManNAc-6P to NanR is crucial for growth (Fig. 5*A*), survival (Fig. 5*B*), and the pathogenesis of *V. vulnificus* (Fig. 5*C*).

V. vulnificus has no genes that are homologs of previously reported neuraminidase genes capable of cleaving sialic acid groups from mucins, but it can obtain free sialic acids from the host in several other ways. First, *V. vulnificus* might possess another type of uncharacterized neuraminidase. Second, the neuraminidases secreted by the normal gut flora may release free sialic acids from the gut mucin glycoprotein or layers. Third, free sialic acids (0.5–3 μM) are present in the serum, although most serum sialic acids are glycoproteins (2 mM) and lipid-associated (10–50 μM) forms (29).

Vibrio pathogenicity island 2, a 57-kb integrative element found exclusively in pathogenic strains of *V. cholerae*, contains a *nan–nag* operon that encodes a cluster of genes involved with the transport and catabolism of sialic acid (30). The *ripR* gene (the gene encoding for ribose phosphate isomerase regulator) in this cluster has been predicted to encode a repressive regulator (11). The *V. cholerae* (O1 biovar El Tor strain N16961) ripR protein shares 79% identity with *V. vulnificus* NanR (*SI Appendix*, Fig. S9), and it may use a similar mechanism to regulate the catabolism of Neu5Ac. The residues that interact with DNA are strictly conserved between the strains, specifically R57 and R60 on α5, and the ManNAc-6P–binding residues, particularly R71, A137, S138, H163, S181, S182, S183, T187, E229, P231, G235, and K240 (*SI Appendix*, Fig. S9). In *H. influenzae*, the *siaPT* and *nan* operons are regulated by SiaR and its ligand GlcN-6P (19). The binding of GlcN-6P to SiaR increases the affinity of SiaR for DNA and activates the expression of the *nan* genes (19), which suggests that the mechanism regulating the *nan* genes in *H. influenzae* differs from that in *Vibrio* strains. However, the residues critical for DNA binding and ligand binding are conserved in *H. influenzae* and *Vibrio* species (*SI Appendix*, Fig. S9). GlcN-6P lacks the acetyl group found in ManNAc-6P. The backbones of P231 and G234 have a water-mediated interaction with the acetyl group in the *Vibrio* regulator. The corresponding residues in *H. influenzae* are K240 and G243, and the difference in the lysine residue may contribute to the different ligand specificities and DNA-binding properties of the regulator in each species. However, the amino acid sequence alignment (*SI Appendix*, Fig. S9) suggests that the regulators [which contain the C-terminal phosphosugar isomerase (SIS) domain (Fig. 2*B*) of the ribose phosphate isomerase regulator family (31)] of the *nan* genes of pathogenic bacteria may share similar structures. It should be noted that $NanR_{Ec}$ and its orthologs, which are found mainly in enteric bacteria (e.g., *Salmonella* and *Shigella* species), appear to have different structures from the SIS domain-containing regulators. They share low sequence similarity (∼38%) with *V. vulnificus* NanR, and the functional residues required for DNA and ligand binding are not well conserved. They belong to the FadR/GntR (fatty acid metabolism regulator and gluconate operon transcriptional repressor, respectively) family (17).

The catabolic utilization of Neu5Ac is important for bacterial pathogenesis, which was demonstrated by the significantly lower

virulence of the isogenic NanA mutant (12) and ligand-binding-deficient NanR mutant (Fig. 5*C*), so molecules that target NanR may have several advantages over conventional antibiotics as unique antimicrobial reagents. First, such molecules could reduce the growth rate of invading pathogens by preventing the transport and catabolism of their preferred in vivo carbon source, which would help the immune system to eliminate pathogens from the host. Second, the use of antagonists to block the binding of ManNAc-6P to NanR is unlikely to disturb the normal flora of the host because the mechanisms that regulate the *nan* genes in typical commensal bacteria differ from those in *V. vulnificus*. For example, *E. coli* uses Neu5Ac itself as the inducer for the transcription of the *nan* gene (17), whereas *Bacteroides* species do not generate ManNAc-6P as a catabolic intermediate of Neu5Ac (32). In summary, the elucidation of the molecular mechanisms involved with the regulation of the *nan* genes described in this study provides a starting point for the design of antibiotics to target life-threatening *Vibrio* species.

Materials and Methods

Bacterial Strains, Plasmids, and Growth Conditions. The bacterial strains and plasmids used are listed in *SI Appendix*, Table S1. Unless stated otherwise, the *E. coli* and *V. vulnificus* strains were grown at 37 °C in Luria–Bertani (LB) medium and at 30 °C in LB supplemented with 2% (wt/vol) NaCl, respectively. When necessary, antibiotics were added to the medium at the following concentrations: 10 μg/mL chloramphenicol, 100 μg/mL ampicillin, and 100 μg/mL kanamycin for *E. coli*; and 3 μg/mL chloramphenicol, 100 μg/mL

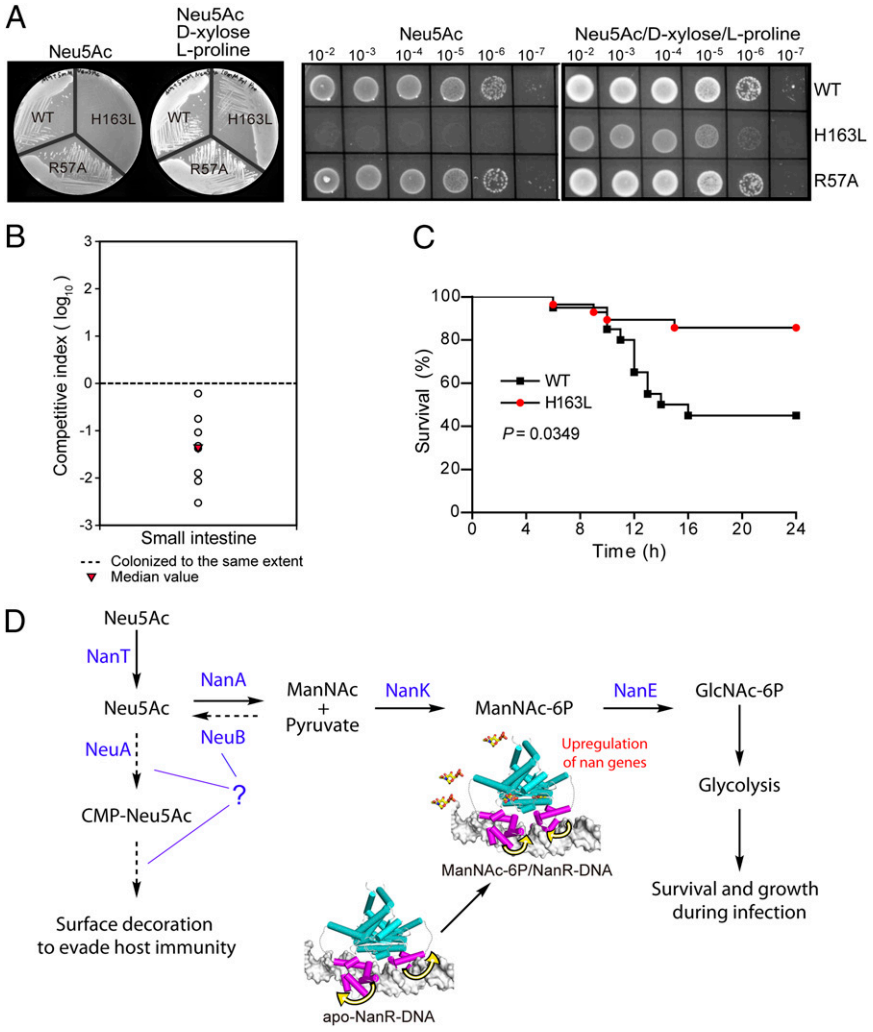

Fig. 5. Importance of the ManNAc-6P–mediated regulation of NanR for bacterial pathogenesis. (*A*) Overnight cultures of WT, R57A, and H163L *V. vulnificus* strains were washed three times with PBS and serially diluted. The undiluted samples were streaked (*Left*), and each dilution was spotted onto M9 minimal medium supplemented with either Neu5Ac alone (*Center*) or Neu5Ac, D-xylose, and L-proline (*Right*). The plates were photographed after 24-h incubation at 30 °C. (*B*) Results of a mouse intestine colonization competition assay using the WT or ligand-binding-defective mutant (H163L) strains. Mice (n = 10) were challenged intragastrically with the bacterial mixture (log phase cells, OD_{600} = 0.6). The competition index was calculated as the ratio of the mutant to WT bacteria recovered from the small intestine. Individual (open circles) and median (red triangle) values are represented as log competitive indices. Two samples produced less than five colonies from the undiluted homogenate, so these data were excluded. (*C*) Survival rates of mice challenged with the WT or H163L strain. Mice (n = 20 per group) were challenged intragastrically with the bacteria (4×10^8 cfu) and monitored for 24 h. Data were pooled from three independent experiments. (*D*) Proposed molecular mechanism of Neu5Ac catabolism via the ManNAc-6P–mediated regulation of NanR. Like the *nan* genes, the genes that encode NeuB and NeuA homologs are found in the *V. vulnificus* genome (VVMO6_02804 and VVMO6_02799). However, it is still unclear whether *V. vulnificus* can synthesize Neu5Ac, then activate and incorporate it into cell surface glycoconjugates (47, 48), so the potential NeuBA pathway is shown with dotted arrows and a question mark. NanR and DNA are shown as ribbon and surface representations, respectively. ManNAc-6P is shown as a ball-and-stick representation. NanT, Neu5Ac transporter; NanA, Neu5Ac lyase; NanK, *N*-acetylmannosamine (ManNAc) kinase; NanE, ManNAc-6P epimerase; NeuB, Neu5Ac synthase; NeuA, CMP–Neu5Ac synthetase.

rifampicin, and 100 μg/mL streptomycin for *V. vulnificus*. M9 minimal medium was supplemented with the appropriate carbon sources (5 mM Neu5Ac alone; or 5 mM Neu5Ac, 10 mM D-xylose, and 10 mM L-proline). ManNAc-6P was purchased from Carbosynth. All other chemicals were purchased from Sigma.

Construction of the Plasmids and Strains. The *nanR* gene was amplified by PCR and cloned into the pGEM-T Easy Vector to generate the pBS1201 construct. Site-directed mutations were introduced into this plasmid by using a QuikChange Site-Directed Mutagenesis Kit (Agilent). The WT or mutant *nanR* genes were then subcloned into the NcoI and XhoI sites of the pBAD-24BS (22) or pHis-parallel1 (33) expression vector to yield the pNB– and pNH– plasmids, respectively. The R57A and H163L mutant *nanR* genes were subcloned into the SphI and SpeI sites of the pDM4 forms pBS1208 and 1209, respectively. To generate the NanR-dependent luciferase promoter–reporter plasmid (pBS0915), the intergenic region between *nanE* and $nanT_P$ was liberated from the pBS0909 plasmid (20) and ligated with BamHI-digested pBBR_lux (34). To construct the *nanR* R57A mutant *V. vulnificus* strain (BS1209) by homologous recombination, *E. coli* conjugal donor strain SM10 λ *pir*,*tra* (containing pBS1208) was mated with wild-type *V. vulnificus* strain MO6-24/O (35). Similarly, *E. coli* SM10 λ *pir*,*tra* strain containing pBS1209 was used as a conjugal donor in conjunction with either MO6-24/O or MORSR (MO6-24/O strain with rifampicin and streptomycin resistance) to generate the *nanR* H163L mutants (BS1210 or BS1213, as indicated in *SI Appendix*, Table S1). The methods used for the conjugation and isolation of the transconjugants were described (20). The lambda Red-recombineering method was used to construct the *nanE*-deletion mutant *E. coli* strain (BSE1201), as described (36). Briefly, the kanamycin resistance (Km^R) cassette from pKD13 was PCR-amplified and electroporated into the BW25113 strain, which contained pKD46. The insertion of the Km^R cassette into *nanE* was confirmed by PCR, and the cassette was subsequently removed from the chromosome by transforming pCP20 into kanamycin-resistant cells. After verifying the deletion of *nanE* by PCR, the cells were maintained at 37 °C for plasmid curing.

***E. coli* Dual Plasmid System.** *E. coli* strains were cotransformed with a luciferase reporter plasmid (pBS0915) and one of the pNB series of plasmids that express NanR. The cells were cultured overnight, diluted with the appropriate fresh medium (supplemented M9 in Fig. 2; LB in Fig. 3) containing arabinose (0.002%), and incubated at 37 °C until the cells reached the early exponential phase. The relative luminescence unit was calculated by dividing the luminescence by the A_{600}, as described (22). To screen the ligand-sensing residues, the BSE1201 strain (*ΔaraBAD ΔnanE*) was used as the host cell instead of DH5α, which ensured that arabinose was not used as a carbon source and that the ManNAc-6P generated from Neu5Ac was accumulated within the cell.

In Vitro Transcription Assay and Quantitative RT-PCR. In vitro transcription assays with WT or mutant NanR proteins were performed according to published procedures (20). The RNA extraction, cDNA synthesis, and real-time PCR amplification of cDNA were performed as described (20).

In Vitro Growth Defects and Mouse Experiments. MO6-24/O (WT), BS1209 (R57A mutant), and BS1210 (H163L mutant) strains were cultured overnight before serial dilution using PBS. Ten microliters of each dilution were spotted onto M9 minimal medium supplemented with 5 mM Neu5Ac only or with 5 mM Neu5Ac, 10 mM D-xylose, and 10 mM L-proline. The growth and phenotypes of the strains were evaluated after incubating at 30 °C for 24 h. In the mouse intestine colonization competition assay, 10 six-week-old female ICR (CD-1) mice were provided with drinking water containing rifampin (50 μg/mL) for 24 h to eliminate resident bacteria (12). After a starvation period without food and water, the mice were infected intragastrically with a bacterial mixture of MORR (WT; Rif^R) and BS1213 (H163L mutant; Rif^R, Sm^R) ($\sim 1 \times 10^6$ cfu per strain). At 12 h postinfection, the mice were euthanized, and the small intestines were collected and homogenized in 5 mL of PBS. Equal amounts of neat or diluted homogenates were spread onto LB agar supplemented with 2% (wt/vol) NaCl and either rifampicin alone to count the sum of WT and H163L mutant cells or rifampicin and streptomycin to count the H163L mutant cells only. The competitive index was calculated by dividing the recovered mutant/WT ratio by the inoculated mutant/WT ratio. In the mouse survival test, 20 mice per group were infected intragastrically with 4×10^8 cfu of either MO6-24/O (WT) or BS1210 (H163L mutant) strains and monitored for 1 d. All animal experiments were performed according to the recommended procedures for the care and use of laboratory animals in the Institute of Laboratory Animal Resources at Seoul National University. The protocol was approved by the Committee on the Ethics of Animal Experiments of Seoul National University (Institutional Animal Care and Use Committee approval no. SNU-111130-2).

Western Blot, EMSA, and DNaseI Footprinting Assay. Purified His–NanR protein was used to raise a primary polyclonal antibody by immunizing European rabbits (*Oryctolagus curiculus*) with a primary injection that contained 500 μg of protein, followed by three boosters that contained 200 μg of protein at 2-wk intervals. Western blotting was performed as described (22). The EMSA and DNaseI footprinting assays were performed according to published procedures (20).

Protein Expression and Purification. The expression and purification of the NanR protein followed published methods (20). The selenomethionine (SeMet)-substituted NanR protein was expressed in the methionine auxotroph *E. coli* B834 (DE3) strain (Novagen), which was grown in minimal medium supplemented with 50 mg/mL SeMet in the same conditions as those used for the expression of native NanR protein. The procedure used for the purification of SeMet-substituted NanR was identical to that used for native NanR, except for the addition of 5 mM methionine to all buffers.

Crystallization, Diffraction, and Structure Determination. The crystallization trials of purified NanR protein using the sitting-drop vapor-diffusion method at 21 °C were unsuccessful. However, crystals were obtained when NanR and ManNAc-6P were mixed in a 1:100 molar ratio and incubated on ice for 2 h. Crystal production was optimized in the following conditions: 10% PEG 2000 monomethyl ether (MME), 0.1 M ammonium sulfate, 0.3 M sodium formate, 3% poly-γ-glutamic acid low molecular weight polymer (PGA-LM), and 0.1 M sodium acetate (pH 5.0–5.5). The crystals appeared within a day and were grown for a further 5 d for diffraction experiments. The complex crystals were transferred to a cryoprotectant solution, which contained 10% PEG 2000 MME, 0.1 M ammonium sulfate, 0.3 M sodium formate, 3% PGA-LM, 0.1 M sodium acetate (pH 5.5), and 30% glycerol, then placed immediately in a −173 °C nitrogen gas stream. The diffraction data for the complex crystals were collected at 1.9-Å resolution. The SeMet-substituted complex crystals were grown in the same crystallization conditions. Single-wavelength anomalous diffraction data for the SeMet-substituted crystals were collected at 2.4-Å resolution. All data were processed by using the HKL2000 package (37). The structure of the NanR/ManNAc-6P complex was determined by analyzing the anomalous signals from Se atoms using the SOLVE program (38). Density modification and subsequent automated model building were performed by using the RESOLVE program (39). The complex crystal structure was solved at 1.9-Å resolution by molecular replacement using the MOLREP program (40) based on the partially refined model of the SeMet crystal. The complex crystal structure was revised by using the COOT program (41) and refined by using REFMAC5 (42). The refinement process included the translation-liberation-screw procedure. The final refined model had R_{free} and R_{cryst} values of 0.235 and 0.183, respectively. No density was visible for the Met-1 to Lys-5 and Glu-82 to Glu-90 regions of NanR-A, as well as the Met-1 to Lys-5, Thr-81 to Gly-91, and Asn-278 regions of NanR-B. Thus, these residues were not included in the model. The model contained 525 amino acid residues, 2 ManNAc-6P molecules, and 221 water molecules, and it satisfied the quality criteria limits of the PROCHECK program (43). The crystallographic data statistics are summarized in Table 1.

Electron Microscopy and Single Particle Analysis. Purified NanR, the NanR/ligand complex, and the NanR/DNA complex were diluted to a final concentration of 300 nM with 50 mM Tris·HCl (pH 7.0) and 300 mM NaCl. Five microliters of the sample solution were applied to a carbon-coated grid, which had been glow-discharged (Harrick Plasma) for 3 min in air, and the grid was negatively stained immediately by using 1% uranyl acetate (44). The grids were examined by using a Technai G2 Spirit Twin transmission electron microscope (FEI) operated at 120 kV, and the images were recorded on a 4K × 4K Ultrascan 895 CCD (Gatan) at a magnification of 0.36 nm/pixel. For the single particle analysis, the images of individual particles were selected interactively in the micrographs, windowed out, and imported into the SPIDER program (Health Research). A total of 894 NanR particles, 1,131 NanR/ligand particles, and 1,039 NanR/DNA particles were used for processing, and the class averages were produced with the reference-free method, as described (45). The datasets were combined, coaligned, and classified to compare similar views of three samples. Class averages with similar views of the NanR region were selected for further analysis. The UCSF Chimera program was used for visualization and comparative analyses of the atomic models and averages (46).

Isothermal Titration Calorimetry. The NanR-binding duplex DNA (5′-gtttgaaaaaaatcttcgttatggattattatggcgatggagattattttcaaac-3′) was chemically synthesized. NanR was dialyzed intensively against Tris buffer (50 mM Tris·HCl, pH 7.0; 300 mM NaCl), and the DNA was diluted to 0.03 mM by using the same buffer. Protein and DNA samples were degassed by

vacuum aspiration for 20 min before loading, and titration was carried out at 25 °C. The NanR dimer was placed in the syringe (0.48 mM) and titrated against the 0.03 mM DNA sample in the reaction cell. The interaction between the NanR/ManNAc-6P complex and the DNA sample was tested by using 0.48 mM complex and 0.03 mM DNA. The calorimetric assays were performed by using a VP-ITC (MicroCal). The stirring speed was 300 rpm, and the thermal power was recorded every 10 s. Raw data were processed and plotted by using the Origin program (Version 7), which was supplied with the instrument.

ACKNOWLEDGMENTS. We thank the beamline staff at Photon Factory, Japan [beamline (BL)-5A and BL-17A], and Pohang Light Source, Korea (BL-4A) for assistance during X-ray diffraction experiments. This work was supported by Global Frontier Project Grant NRF-2010-0029767, funded by the Ministry of Science, ICT, and Future Planning (MSIP) of Korea and the Korea Research Institute of Bioscience and Biotechnology Research Initiative Program (to M.H.K.); Mid-Career Researcher Program Grant 2012R1A2A1A03009679, funded by MSIP and the Research and Development Convergence Center Support Program of the Ministry for Food, Agriculture, Forestry, and Fisheries of Korea (to S.H.C.); and a grant from the Korea Basic Science Institute (T33415 to H.S.J.).

1. Dethlefsen L, McFall-Ngai M, Relman DA (2007) An ecological and evolutionary perspective on human-microbe mutualism and disease. *Nature* 449(7164):811–818.
2. Ley RE, Peterson DA, Gordon JI (2006) Ecological and evolutionary forces shaping microbial diversity in the human intestine. *Cell* 124(4):837–848.
3. Chang DE, et al. (2004) Carbon nutrition of *Escherichia coli* in the mouse intestine. *Proc Natl Acad Sci USA* 101(19):7427–7432.
4. Hooper LV, Midtvedt T, Gordon JI (2002) How host-microbial interactions shape the nutrient environment of the mammalian intestine. *Annu Rev Nutr* 22:283–307.
5. Larsson JM, Karlsson H, Sjövall H, Hansson GC (2009) A complex, but uniform O-glycosylation of the human MUC2 mucin from colonic biopsies analyzed by nanoLC/MSn. *Glycobiology* 19(7):756–766.
6. Wiggins R, Hicks SJ, Soothill PW, Millar MR, Corfield AP (2001) Mucinases and sialidases: Their role in the pathogenesis of sexually transmitted infections in the female genital tract. *Sex Transm Infect* 77(6):402–408.
7. Vimr ER, Kalivoda KA, Deszo EL, Steenbergen SM (2004) Diversity of microbial sialic acid metabolism. *Microbiol Mol Biol Rev* 68(1):132–153.
8. Angata T, Varki A (2002) Chemical diversity in the sialic acids and related alpha-keto acids: An evolutionary perspective. *Chem Rev* 102(2):439–469.
9. Severi E, Hood DW, Thomas GH (2007) Sialic acid utilization by bacterial pathogens. *Microbiology* 153(Pt 9):2817–2822.
10. Vimr ER, Troy FA (1985) Identification of an inducible catabolic system for sialic acids (nan) in *Escherichia coli*. *J Bacteriol* 164(2):845–853.
11. Almagro-Moreno S, Boyd EF (2009) Sialic acid catabolism confers a competitive advantage to pathogenic *Vibrio cholerae* in the mouse intestine. *Infect Immun* 77(9):3807–3816.
12. Jeong HG, et al. (2009) The capability of catabolic utilization of N-acetylneuraminic acid, a sialic acid, is essential for *Vibrio vulnificus* pathogenesis. *Infect Immun* 77(8):3209–3217.
13. Olson ME, King JM, Yahr TL, Horswill AR (2013) Sialic acid catabolism in *Staphylococcus aureus*. *J Bacteriol* 195(8):1779–1788.
14. Mandlik A, et al. (2011) RNA-Seq-based monitoring of infection-linked changes in *Vibrio cholerae* gene expression. *Cell Host Microbe* 10(2):165–174.
15. Almagro-Moreno S, Boyd EF (2009) Insights into the evolution of sialic acid catabolism among bacteria. *BMC Evol Biol* 9:118.
16. Plumbridge J, Vimr E (1999) Convergent pathways for utilization of the amino sugars N-acetylglucosamine, N-acetylmannosamine, and N-acetylneuraminic acid by *Escherichia coli*. *J Bacteriol* 181(1):47–54.
17. Kalivoda KA, Steenbergen SM, Vimr ER, Plumbridge J (2003) Regulation of sialic acid catabolism by the DNA binding protein NanR in *Escherichia coli*. *J Bacteriol* 185(16):4806–4815.
18. Johnston JW, et al. (2007) Regulation of sialic acid transport and catabolism in *Haemophilus influenzae*. *Mol Microbiol* 66(1):26–39.
19. Johnston JW, Shamsulddin H, Miller AF, Apicella MA (2010) Sialic acid transport and catabolism are cooperatively regulated by SiaR and CRP in nontypeable *Haemophilus influenzae*. *BMC Microbiol* 10:240.
20. Kim BS, Hwang J, Kim MH, Choi SH (2011) Cooperative regulation of the *Vibrio vulnificus* nan gene cluster by NanR protein, cAMP receptor protein, and N-acetylmannosamine 6-phosphate. *J Biol Chem* 286(47):40889–40899.
21. Teplyakov A, Obmolova G, Badet B, Badet-Denisot MA (2001) Channeling of ammonia in glucosamine-6-phosphate synthase. *J Mol Biol* 313(5):1093–1102.
22. Kim Y, et al. (2010) Crystal structure of SmcR, a quorum-sensing master regulator of *Vibrio vulnificus*, provides insight into its regulation of transcription. *J Biol Chem* 285(18):14020–14030.
23. Aravind L, Anantharaman V, Balaji S, Babu MM, Iyer LM (2005) The many faces of the helix-turn-helix domain: Transcription regulation and beyond. *FEMS Microbiol Rev* 29(2):231–262.
24. Karlsson KA (1998) Meaning and therapeutic potential of microbial recognition of host glycoconjugates. *Mol Microbiol* 29(1):1–11.
25. Vimr E, Lichtensteiger C (2002) To sialylate, or not to sialylate: That is the question. *Trends Microbiol* 10(6):254–257.
26. Martinez J, Steenbergen S, Vimr E (1995) Derived structure of the putative sialic acid transporter from *Escherichia coli* predicts a novel sugar permease domain. *J Bacteriol* 177(20):6005–6010.
27. Almagro-Moreno S, Boyd EF (2010) Bacterial catabolism of nonulosonic (sialic) acid and fitness in the gut. *Gut Microbes* 1(1):45–50.
28. Ross W, Ernst A, Gourse RL (2001) Fine structure of *E. coli* RNA polymerase-promoter interactions: Alpha subunit binding to the UP element minor groove. *Genes Dev* 15(5):491–506.
29. Sillanaukee P, Pönniö M, Jääskeläinen IP (1999) Occurrence of sialic acids in healthy humans and different disorders. *Eur J Clin Invest* 29(5):413–425.
30. Jermyn WS, Boyd EF (2002) Characterization of a novel *Vibrio* pathogenicity island (VPI-2) encoding neuraminidase (nanH) among toxigenic *Vibrio cholerae* isolates. *Microbiology* 148(Pt 11):3681–3693.
31. Bateman A (1999) The SIS domain: A phosphosugar-binding domain. *Trends Biochem Sci* 24(3):94–95.
32. Brigham C, et al. (2009) Sialic acid (N-acetyl neuraminic acid) utilization by Bacteroides fragilis requires a novel N-acetyl mannosamine epimerase. *J Bacteriol* 191(11):3629–3638.
33. Sheffield P, Garrard S, Derewenda Z (1999) Overcoming expression and purification problems of RhoGDI using a family of "parallel" expression vectors. *Protein Expr Purif* 15(1):34–39.
34. Lenz DH, et al. (2004) The small RNA chaperone Hfq and multiple small RNAs control quorum sensing in *Vibrio harveyi* and *Vibrio cholerae*. *Cell* 118(1):69–82.
35. Miller VL, Mekalanos JJ (1988) A novel suicide vector and its use in construction of insertion mutations: Osmoregulation of outer membrane proteins and virulence determinants in *Vibrio cholerae* requires toxR. *J Bacterial* 170(6):2575–2583.
36. Datsenko KA, Wanner BL (2000) One-step inactivation of chromosomal genes in *Escherichia coli* K-12 using PCR products. *Proc Natl Acad Sci USA* 97(12):6640–6645.
37. Otwinowski Z, Minor W (1997) Processing of x-ray diffraction data collected in oscillation mode. *Methods Enzymol* 276:307–326.
38. Terwilliger TC, Berendzen J (1997) Bayesian correlated MAD phasing. *Acta Crystallogr D Biol Crystallogr* 53(Pt 5):571–579.
39. Terwilliger TC (2001) Maximum-likelihood density modification using pattern recognition of structural motifs. *Acta Crystallogr D Biol Crystallogr* 57(Pt 12):1755–1762.
40. Vagin A, Teplyakov A (1997) MOLREP: An automated program for molecular replacement. *J Appl Cryst* 30:1022–1025.
41. Emsley P, Cowtan K (2004) Coot: Model-building tools for molecular graphics. *Acta Crystallogr D Biol Crystallogr* 60(Pt 12 Pt 1):2126–2132.
42. Murshudov GN, Vagin AA, Dodson EJ (1997) Refinement of macromolecular structures by the maximum-likelihood method. *Acta Crystallogr D Biol Crystallogr* 53(Pt 3):240–255.
43. Laskowski RA, Moss DS, Thornton JM (1993) Main-chain bond lengths and bond angles in protein structures. *J Mol Biol* 231(4):1049–1067.
44. Jung HS, Komatsu S, Ikebe M, Craig R (2008) Head-head and head-tail interaction: A general mechanism for switching off myosin II activity in cells. *Mol Biol Cell* 19(8):3234–3242.
45. Jung HS, et al. (2008) Conservation of the regulated structure of folded myosin 2 in species separated by at least 600 million years of independent evolution. *Proc Natl Acad Sci USA* 105(16):6022–6026.
46. Pettersen EF, et al. (2004) UCSF Chimera—a visualization system for exploratory research and analysis. *J Comput Chem* 25(13):1605–1612.
47. Lewis AL, et al. (2009) Innovations in host and microbial sialic acid biosynthesis revealed by phylogenomic prediction of nonulosonic acid structure. *Proc Natl Acad Sci USA* 106(32):13552–13557.
48. Lewis AL, et al. (2011) Genomic and metabolic profiling of nonulosonic acids in Vibrionaceae reveal biochemical phenotypes of allelic divergence in *Vibrio vulnificus*. *Appl Environ Microbiol* 77(16):5782–5793.